Comput Mech
DOI 10.1007/s00466-008-0346-3

ORIGINAL PAPER

Benchmark problems for wave propagation in elastic materials

A. Idesman · H. Samajder · E. Aulisa · P. Seshaiyer

Received: 13 May 2008 / Accepted: 20 October 2008

Abstract The application of the new numerical approach for elastodynamics problems developed in our previous paper and based on the new solution strategy and the new time-integration methods is considered for 1D and 2D axi-symmetric impact problems. It is not easy to solve these problems accurately because the exact solutions of the corresponding semi-discrete elastodynamics problems contain a large number of spurious high-frequency oscillations. We use the 1D impact problem for the calibration of a new analytical expression describing the minimum amount of numerical dissipation necessary for the new time-integration method used for filtering spurious oscillations. Then, we show that the new numerical approach for elastodynamics along with the new expression for numerical dissipation for the first time yield accurate and non-oscillatory solutions of the considered impact problems. The comparison of effectiveness of linear and quadratic elements as well as rectangular and triangular finite elements for elastodynamics problems is also considered.

Keywords Wave · Damping · Finite element

A. Idesman (✉) · H. Samajder
Department of Mechanical Engineering,
Texas Tech University,
Lubbock, TX 79409-1021, USA
e-mail: alexander.idesman@ttu.edu

H. Samajder
e-mail: himadri.samajder@ttu.edu

E. Aulisa
Department of Mathematics and Statistics,
Texas Tech University, Broadway and Boston,
Lubbock, TX 79409-1042, USA
e-mail: eugenio.aulisa@ttu.edu

P. Seshaiyer
Department of Mathematical Sciences,
George Mason University, 4400 University Drive,
MS: 3F2, Science and Tech I, Fairfax, VA 22030, USA
e-mail: pseshaiy@gmu.edu

1 Introduction

Despite a large number of publications related to numerical methods for non-linear elastodynamics problems, there is no reliable numerical technique for an accurate non-oscillatory solution of wave propagation problems, even for linear elastic materials. In effect, it means that one cannot trust the numerical results obtained for wave propagation problems in solids. Let us analyze the issues with existing numerical methods for elastodynamics in greater detail. Most finite element procedures for elastodynamics problems are based upon semi-discrete methods [5–7,19,20,23,25]. For these methods, the application of finite elements in space to linear elastodynamics problems leads to a system of ordinary differential equations in time

$$\boldsymbol{M}\ddot{\boldsymbol{U}} + \boldsymbol{C}\dot{\boldsymbol{U}} + \boldsymbol{K}\boldsymbol{U} = \boldsymbol{R}. \tag{1}$$

Here $\boldsymbol{M}, \boldsymbol{C}, \boldsymbol{K}$ are the mass, damping, and stiffness matrices, respectively, $\boldsymbol{U}$ is the vector of the nodal displacement, $\boldsymbol{R}$ is the vector of the nodal load. Equation (1) can be also obtained by the application of other discretization methods in space such as the finite difference method, the spectral element method, the boundary element method, the smoothed particle hydrodynamics (SPH) method and others. Many different numerical methods have been developed for the time integration of Eq. 1.

However, for wave propagation problems, the integration of Eq. 1 leads to the appearance of spurious high-frequency oscillations. Both the spatial discretization used for the

derivation of Eq. 1, and the time integration of Eq. 1 affect spurious oscillations and the accuracy of a numerical solution. There are no reliable numerical methods that yield an accurate solution without spurious oscillations. Current numerical approaches that treat this issue are based on the introduction of numerical dissipation or artificial viscosity from the first time increment for the suppression of spurious high-frequency oscillations; see [1–8,15–20,22–25] and others. However, numerical dissipation or artificial viscosity also affects low modes of a numerical solution. Although this effect is small for a small number of time increments, due to error accumulation during the time integration of Eq. 1, low modes of numerical solutions become very inaccurate even at a moderate number of time increments. If numerical dissipation is not used in calculations, then spurious high-frequency oscillations spoil the numerical solution. The existing methods with numerical dissipation or artificial viscosity do not take into account the effect of the number of time increments on the accuracy of final numerical results. Therefore, different researchers report different values of artificial viscosity needed for the suppression of spurious oscillations (e.g., see the recent paper [24] and references there), and it is not clear what the optimal value of artificial viscosity is or how to select it (there is no understanding that this value depends on the number of time increments). And even if spurious oscillations are suppressed for a specific number of time increments, the final solution will be inaccurate due to error accumulation at low modes. *This contradiction between the accuracy of low modes and the suppression of spurious high-frequency oscillations cannot be resolved within the existing approaches.*

Recently we suggested a new numerical technique that yields non-oscillatory, accurate and reliable solutions for wave propagation in solids; see [11,13]. The technique is based on a new solution strategy and new first-, second- and high-order accurate time-integration methods for elastodynamics. In this paper we will study and specify some algorithmic parameters of the new technique using numerical experiments with 1D and 2D impact problems. Numerical solutions to these problems obtained by the integration of Eq. 1 with the trapezoidal rule (without numerical dissipation) contain a large number of spurious high-frequency oscillations which must be removed without damage to low-frequency modes. Therefore, these problems can be used as benchmark problems for the development of new accurate non-oscillatory numerical methods for wave propagation in elastic materials. The paper includes a short description of the new numerical technique based on the new two-stage solution strategy for elastodynamics and the new first-order time-continuous Galerkin (TCG) implicit method used for filtering spurious high-frequency oscillations. This technique has been developed in our previous papers; see [11,13]. Applying the new approach to the solution of a 1D impact problem, we will determine an analytical expression for the necessary amount of numerical dissipation (in terms of the size of a time increment) which should be used for filtering spurious high-frequency oscillations with the new first-order TCG method. The necessary amount of numerical dissipation depends on the number of time increments, on the observation time, and on the dimensions of linear and quadratic finite elements. Finally, we will show that the new numerical technique combined with the new formula yields accurate and non-oscillatory numerical results for 1D and multi-dimensional wave propagation problems. The effectiveness of the application of quadrilateral and triangular 2D finite elements with different aspect ratios to wave propagation problems is compared. In contrast to existing approaches, the new technique for the first time allows a reliable, fast, accurate and non-oscillatory solution of wave propagation in solids and does not require any guesswork for the selection of numerical dissipation or artificial viscosity.

2 Numerical technique

The new two-stage solution strategy and the new TCG methods suggested in [11–13] will be used in order to resolve the seemingly irresolvable contradiction of current approaches to filtering spurious oscillations. The main advantages of the new approach are as follows; see [13]. The new numerical technique: (a) allows the selection of the best numerical method for basic computations according to simple criteria (the most important one being the accuracy of the method); (b) includes pre- or post-processing for filtering spurious high-frequency oscillations, which requires little computation time compared to the stage of basic computations (a small number of time increments with the new implicit TCG method with large numerical dissipation is used for pre- or post-processing); (c) yields no error accumulation due to numerical dissipation (or artificial viscosity) during time integration at the stage of basic computations; (d) does not require any guesswork for the selection of numerical dissipation or artificial viscosity as do existing approaches. Thus, the approach can be easily incorporated in computer codes and does not require interaction with users for the suppression of spurious high-frequency oscillations. Below we briefly describe the new solution strategy for elastodynamics, and the new first-order implicit TCG method with large numerical dissipation that, according to the new strategy, is used for filtering spurious oscillations (see [11–13] for a detailed description).

2.1 A new two-stage solution strategy for elastodynamics

The idea of the new two-stage strategy is very simple. Because for linear elastodynamics problems there is no interaction between different modes during time integration (they are

integrated independently of one another), the most accurate time-integration method (without numerical dissipation or artificial viscosity) should be used for the basic computations of Eq. 1, especially for a long-term integration. It means that all modes (including high-frequency modes) are integrated very accurately and the solution includes spurious high-frequency oscillations. Then, for the damping out of high modes, a method with large numerical dissipation (or with artificial viscosity) is used for a number of time increments as a pre- or post-processor. This method can be considered a filter of high modes. Usually, a small number of time increments is sufficient for the filtering stage, with negligible error accumulation at low modes. Therefore, even a time-integration method of the first order of accuracy is competitive at this stage.

Remark The proposed procedure has common features with the modal decomposition method [1,8]. If all modes are used, then the modal decomposition method yields the same results as does the accurate time integration of a semi-discrete system Eq. 1. However, it is known that accurate numerical results can be obtained by modal decomposition with a limited number of low modes. The application of numerical dissipation for pre- or post-processing in the suggested procedure is partly equivalent to removing a number of high modes from the numerical results for which all modes are included. It means that this approach is partly equivalent to the modal decomposition method (without the necessity of calculations of the eigenvalues and eigenvectors of a semi-discrete system, Eq. 1).

In the current paper, we will use the implicit second-order accurate trapezoidal rule for basic computations in order to obtain an accurate solution of the semi-discrete elastodynamics problem, Eq. 1 (this solution contains spurious high-frequency oscillations). We should mention that other known methods such as the explicit central difference method (the second-order time-integration method with zero numerical dissipation) or high-order implicit and explicit methods can also be used for basic computations. All these methods yield the same results for the time integration of Eq. 1 at relatively small time increments. The selection of the trapezoidal rule for basic computations is related to its high accuracy (the trapezoidal rule is the most accurate method among all second-order time integration methods) and simplicity of implementation. For filtering spurious oscillations, the new first-order implicit TCG method with large numerical dissipation, developed in [13] and briefly described below, is used.

2.2 The first-order implicit TCG method for filtering spurious high-frequency oscillations

For the step-by-step integration procedure with a time increment Δt, the linear approximations of displacements $U(t)$ and velocities $V(t)$ within a time increment Δt ($0 \le t \le \Delta t$) are used for the new TCG method (see [13])

$$\boldsymbol{U}(t) = \boldsymbol{U}_0 + \boldsymbol{U}_1 t, \quad \boldsymbol{V}(t) = \boldsymbol{V}_0 + \boldsymbol{V}_1 t, \tag{2}$$

where $\boldsymbol{U}_0$ and $\boldsymbol{V}_0$ are the known initial nodal displacements and velocities. The unknown nodal vector $\boldsymbol{V}_1$ can be expressed in terms of the unknown nodal vector $\boldsymbol{U}_1$ as follows:

$$\boldsymbol{V}_1 = \frac{1}{a_1}\boldsymbol{U}_1 - \frac{1}{a_1}\boldsymbol{V}_0 . \tag{3}$$

Finally, the following system of algebraic equations is solved for the determination of $\boldsymbol{U}_1$

$$(\boldsymbol{M} + a_1\boldsymbol{C} + a_1^2\boldsymbol{K})\boldsymbol{U}_1 = -a_1\boldsymbol{K}\boldsymbol{U}_0 + \boldsymbol{M}\boldsymbol{V}_0 + \boldsymbol{R}_1 , \tag{4}$$

where

$$a_1 = \frac{m+2}{m+3}\Delta t , \tag{5}$$

$$\boldsymbol{R}_1 = \frac{(m+2)^2}{(m+3)\Delta t^{m+1}} \int_0^{\Delta t} \boldsymbol{R}(t) t^{m+1}\, dt . \tag{6}$$

The parameter m is responsible for the amount of numerical dissipation. After the calculation of $\boldsymbol{U}_1$ from Eq. 4, the values of displacements and velocities at the end of a time increment Δt are calculated using Eqs. (2) and (3) for $t = \Delta t$; i.e.,

$$\boldsymbol{U}(\Delta t) = \boldsymbol{U}_0 + \boldsymbol{U}_1 \Delta t , \tag{7}$$

$$\boldsymbol{V}(\Delta t) = \left(1 - \frac{1}{a_1}\right)\boldsymbol{V}_0 = \frac{1}{a_1}\boldsymbol{U}_1 \Delta t . \tag{8}$$

According to the accuracy analysis, the method has the first order of accuracy in time. The spectral radii of the amplification matrix for the implicit TCG method are shown in Fig. 1 for different values of m. The algorithmic damping ratios and the relative period errors are given in Fig. 2. It can been seen from Fig. 1 that the spectral radius decreases (numerical dissipation increases) with the increase in the parameter m. The maximum numerical dissipation corresponds to $m = \infty$. For

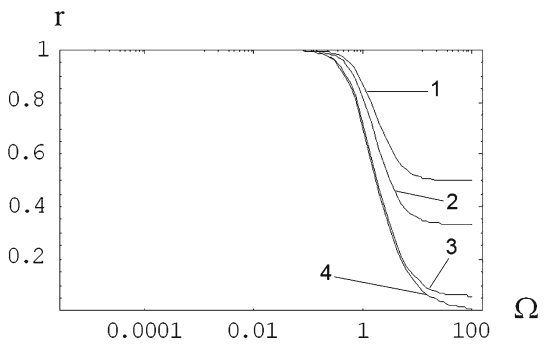

Fig. 1 Spectral radii r for the first-order implicit TCG method with large numerical dissipation. Curves 1, 2, 3, and 4 correspond to $m = 0, 1, 15, \infty$, respectively

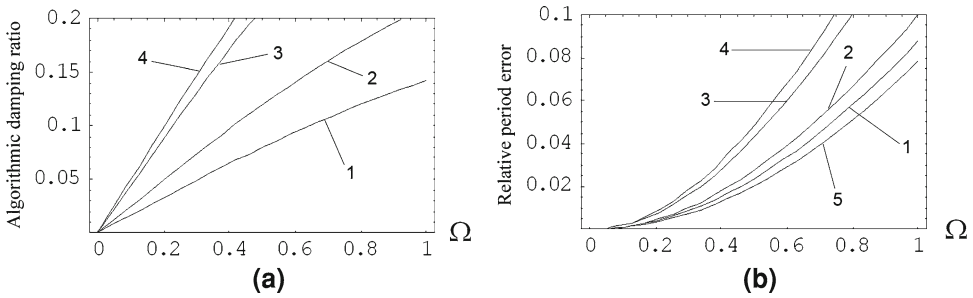

Fig. 2 Algorithmic damping ratios and relative period errors for the first-order implicit TCG method with large numerical dissipation. Curves 1, 2, 3, 4, and 5 correspond to $m = 0, 1, 15, \infty$ and the trapezoidal rule, respectively

the case $m = \infty$, the parameter $a_1 = \Delta t$, and $\boldsymbol{R}_1$ should be calculated analytically; see Eq. 6. If the analytical calculation of $\boldsymbol{R}_1$ at $m = \infty$ is impossible, then a value $m \geq 15$ can be used, because the difference in numerical dissipation for $m = \infty$ and $m \geq 15$ is not very essential ($m = 15$ is used in calculations in this paper). The numerical examples show that the first-order accurate implicit TCG method allows the suppression of spurious high-frequency oscillations for a small number of time increments while retaining good accuracy of the solution at low modes (see below). $\boldsymbol{C} = \boldsymbol{0}$ (no viscosity) is used for the problems considered below.

3 Numerical modeling

The new technique based on the new two-stage solution strategy and the new first-order implicit TCG method are implemented into the finite element code FEAP [25]. Two impact problems in the 1D and 2D axisymmetric cases will be considered in the paper. These problems include propagation of discontinuities in stresses and velocities and cannot be accurately solved by the existing methods based on the introduction of artificial viscosity (or numerical dissipation) at each time increment. We will use the first 1D impact problem, which has an analytical solution, for:

- the calibration of the minimum necessary amount of numerical dissipation for the new first-order TCG method with large numerical dissipation. A new analytical expression for numerical dissipation in terms of the size of a time increment will be suggested for linear and quadratic finite elements;
- the selection of the number of time increments needed for the filtering of spurious high-frequency oscillations by the new first-order TCG method with large numerical dissipation;
- the comparison of effectiveness of linear and quadratic finite elements for wave propagation problems.

The second 2D impact axisymmetric problem, which includes simultaneous propagation of longitudinal and transverse elastic waves and for which an approximate analytical solution is known from the literature [21], will be used for

- verification of the applicability of the new formula for the minimum necessary amount of numerical dissipation derived in the 1D case for the multi-dimensional case. In contrast to the 1D case with propagation of only longitudinal waves, simultaneous propagation of longitudinal and transverse elastic waves occurs in the multi-dimensional case;
- comparison of effectiveness of linear and quadratic finite elements for wave propagation problems in the multi-dimensional case;
- comparison of effectiveness of quadrilateral and triangular finite elements for wave propagation problems in the multi-dimensional case;
- study of the effect of the aspect ratio of 2D quadrilateral finite elements on the accuracy of numerical results for wave propagation problems.

3.1 Impact of an elastic bar against a rigid wall

3.1.1 Problem formulation

The first 1D problem is related to the impact of an elastic bar of the length $L = 4$ against a rigid wall (see Fig. 3). Young's modulus is chosen to be $E = 1$ and the density to be $\rho = 1$. The following boundary conditions are applied: the displacement $u(0, t) = t$ (which corresponds to the velocity $v(0, t) = v_0 = 1$) and $u(4, t) = 0$ (which corresponds to the velocity $v(4, t) = 0$). Initial displacements and velocities are zero; i.e., $u(x, 0) = v(x, 0) = 0$. The problem has the continuous solution for displacements $u_a(x, t) = t - x$ for $t \geq x$ and $u_a(x, t) = 0$ for $t \leq x$, and the discontinuous solution for velocities and stresses $v_a(x, t) = -\sigma^a(x, t) = 1$ for $t \geq x$ and $v_a(x, t) = \sigma^a(x, t) = 0$ for $t \leq x$ (at the interface $x = t$, jumps in stresses and velocities occur).

It is known that the application of traditional semi-discrete methods to this problem leads to oscillations in velocities and stresses due to the spurious high-frequency response [9–12]. This impact problem with propagating discontinuities in stresses and velocities can be considered a good benchmark problem for the testing of new numerical methods for wave propagation problems.

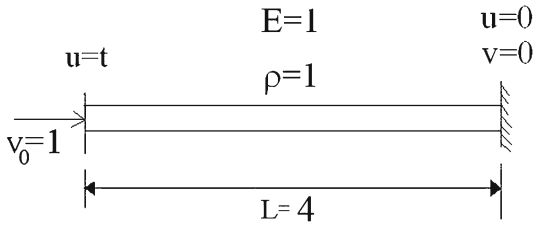

Fig. 3 Impact of an elastic bar of length $L = 4$ against a rigid wall

It was shown in [13] that the new solution strategy combined with the new first-order implicit TCG method yields an accurate and non-oscillatory solution to the 1D impact problem considered. However, the detailed study related to the selection of the necessary amount of numerical dissipation for filtering spurious oscillations has not been considered in [13]. Below we will use the 1D impact problem for the calibration of the minimum amount of numerical dissipation needed in the new first-order TCG method to filter spurious oscillations as well as for the study of the effectiveness of the new solution strategy in combination with the new time-integration TCG method.

3.1.2 Determination of the minimum amount of numerical dissipation necessary for filtering spurious oscillations

The following empirical formula for the selection of the size of a time increment for a time-integration method with large numerical dissipation has be suggested in [13]:

$$\Delta t = \alpha(N_1)\frac{\Delta x \Omega_{0.1}(N)}{c}, \tag{9}$$

where $c = \sqrt{\frac{E}{\rho}}$ is the wave velocity; Δx is the size of a finite element; $\Omega_{0.1}(N)$ is the value of $\Omega = w\Delta t$ at which the spectral radius has the value 0.1 for the selected number N of time increments (see [13]); $\Omega_{0.1}$ is used to scale spectral radii calculated at different numbers of time increments N; $\alpha(N_1)$ is the empirical coefficient depending on the time-integration method, on the order of finite elements, and on the number N_1 of elements which are passed through by the wave front (this number can be expressed as $N_1 = \frac{cT}{\Delta x}$). This formula yields the minimum necessary amount of numerical dissipation (in terms of the size of a time increment), which depends on the number of time increments N (through the parameter $\Omega_{0.1}(N)$) used for filtering spurious oscillations, on the observation time T and on the dimension of a finite element Δx (uniform meshes are assumed).

Remark 1 It should be mentioned that at a given number N of time increments, two parameters $\alpha(N_1)$ and $\Omega_{0.1}(N)$ in Eq. (9) can be combined into one parameter $\bar{\alpha}(N_1)$; i.e., at different N the empirical coefficient $\bar{\alpha}(N_1)$ can be determined from numerical experiments. However, we reduce the number of numerical experiments using the analytical scaling of the spectral radii at different N. For the scaling, a point with the value of the spectral radius $r = 0.1$ on the transient part of the spectral radius diagrams is used. According to numerical experiments, Eq. (9) with the scaling coefficient $\Omega_{0.1}(N)$ calculated analytically from the spectral radius diagram, yields a good approximation for the selection of numerical dissipation at different N.

Remark 2 Equation (9) is based on the following idea. By the use of the dimensionless coordinates, it is easy to show that the solution of Eq. (1) for the 1D impact problem on a uniform mesh depends only on the number of elements N_1 passed by the wave front and is independent of the size of elements, the observation time and material properties (we also use the assumption that the solution is independent of the total number of elements of a finite element mesh; see Fig. 10). Then, the numerical dissipation needed for the suppression of spurious oscillations for the 1D impact problems depends on the same parameter N_1. Equation (9) shows that a non-dimensionless time increment $\frac{\Delta t c}{\Delta x}$ is a function of the parameter N_1; see [13].

In order to apply Eq. (9) in calculations, we will describe a procedure used for the analytical approximation of the coefficient $\alpha(N_1)$ in Eq. (9). For this procedure we will use the new solution strategy based on the basic computations and following post-processing with the new first-order method TCG with large numerical dissipation. $N = 10$ time increments is used for post-processing, therefore $\Omega_{0.1}(N = 10) = 0.81$; see [13] (the effect of the different numbers N for post-processing is studied below as well). The velocity distributions after basic computations at different observation times are shown in Figs. 4a and 5a. Two uniform meshes with 100 linear and 50 quadratic finite elements (i.e., meshes with the same numbers of degrees of freedom) are used for these calculations. The second-order accurate implicit trapezoidal rule is used for basic computations, and the implicit first-order accurate TCG method is used for post-processing. A sufficiently small size of time increments ($\Delta t = 0.00005$) for basic calculations is applied. Therefore, for the selected observation times, the error in time for basic computations is very small and can be neglected for both meshes. From Figs. 4a and 5a it follows that after basic computations the slope of the wave front decreases with the increase in observation time (or more precisely, with the increase in the number of elements passed through by the wave front; see [13]). Similar numerical results were reported in [14]. The amplitude and frequency of spurious oscillations are also different at the different observation times (despite the fact that for the selected observation times the analytical solutions coincide; see curve 5).

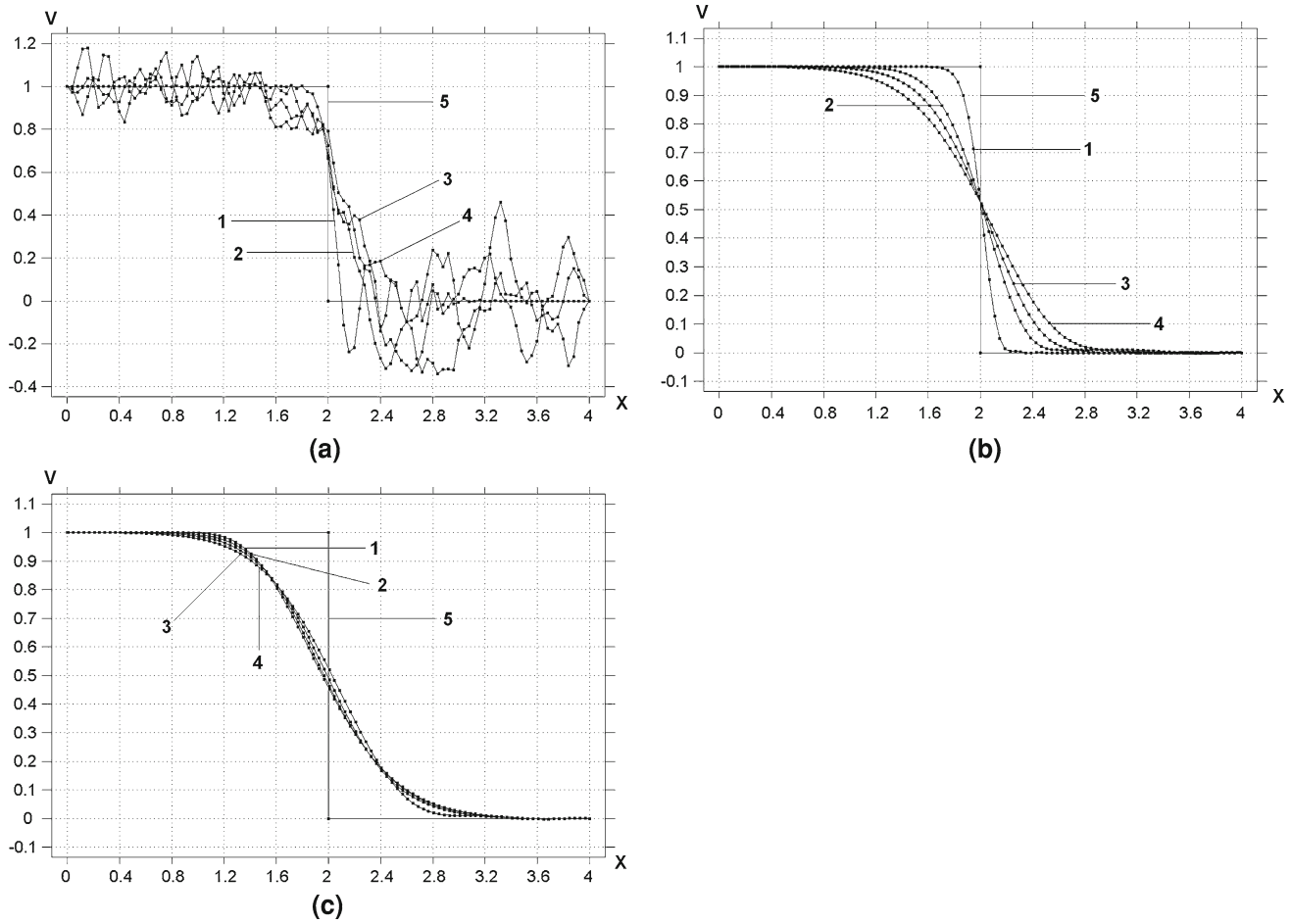

Fig. 4 Velocity distribution along the bar for long-term behavior calculated on a uniform mesh with 100 linear 2-node finite elements. **a**, **b**, **c** correspond to the solutions obtained by the trapezoidal rule, by the new strategy with post-processing based on uniform time increments of different sizes (using varying α) at different observation times, and by the new strategy with post-processing based on uniform time increments of the same sizes (using constant $\alpha = 4.67$) at different observation times; see the text for the explanations. Curves 1, 2, 3 and 4 correspond to the observation times $T = 2, 42, 98$ and 202, respectively. Curve 5 corresponds to the analytical solutions at the observation times $T = 2, 42, 98$ and 202

Next, we will define the measure of spurious oscillations as follows. At each observation time we will find coordinates x_1 and x_2 at which the wave front in a numerical solution for the velocity intersects two horizontal lines corresponding to the analytical solution for velocity $v = 1$ and $v = 0$; see Fig. 6. Then, for each interval $0 \le x \le x_1$ and $x_2 \le x \le 4$ we will find two relative errors $e_1 = (v_1^{\max} - v_1^{\min})/v_{\max}$ and $e_2 = (v_2^{\max} - v_2^{\min})/v_{\max}$, where $v_i^{\max}$ and $v_i^{\min x}$ are the maximum and minimum values of a numerical solution for the velocity at interval i ($i = 1, 2$), and $v_{\max} = 1$ is the maximum value of the velocity from the analytical solution. Finally, we will define the relative error $e = \max(e_1, e_2)$ related to spurious oscillations. It is clear that the smaller e is, the smaller the spurious oscillations are.

The application of the new first-order TCG method with large numerical dissipation decreases the relative error e. At a fixed number of time increments N, this decrease depends on the size of a time increment. By the variation of the size of a time increment Δt for post-processing, we determine from numerical experiments the size of the time increment $\Delta \bar{t}$ at which $e \approx \varepsilon = 0.25\%$ where $\varepsilon = 0.25\%$ is the selected tolerance. The tolerance should be small in order to bound the amplitudes of spurious oscillations.

Remark We should mention that if a time increment is larger than $\Delta \bar{t}$, then numerical dissipation will be larger and the relative error e will be smaller than the selected tolerance ε. However, excessive numerical dissipation also decreases the accuracy of a numerical solution at low modes; i.e., the width of the wave front increases (see Figs. 4b, c and 5b, c and the discussion below). Therefore, only the necessary amount of numerical dissipation (in terms of the size of a time increment) is recommended in calculations for accurate non-oscillatory numerical results.

By the procedure described above, the size of a time increment $\Delta \bar{t}$ was determined from numerical experiments at

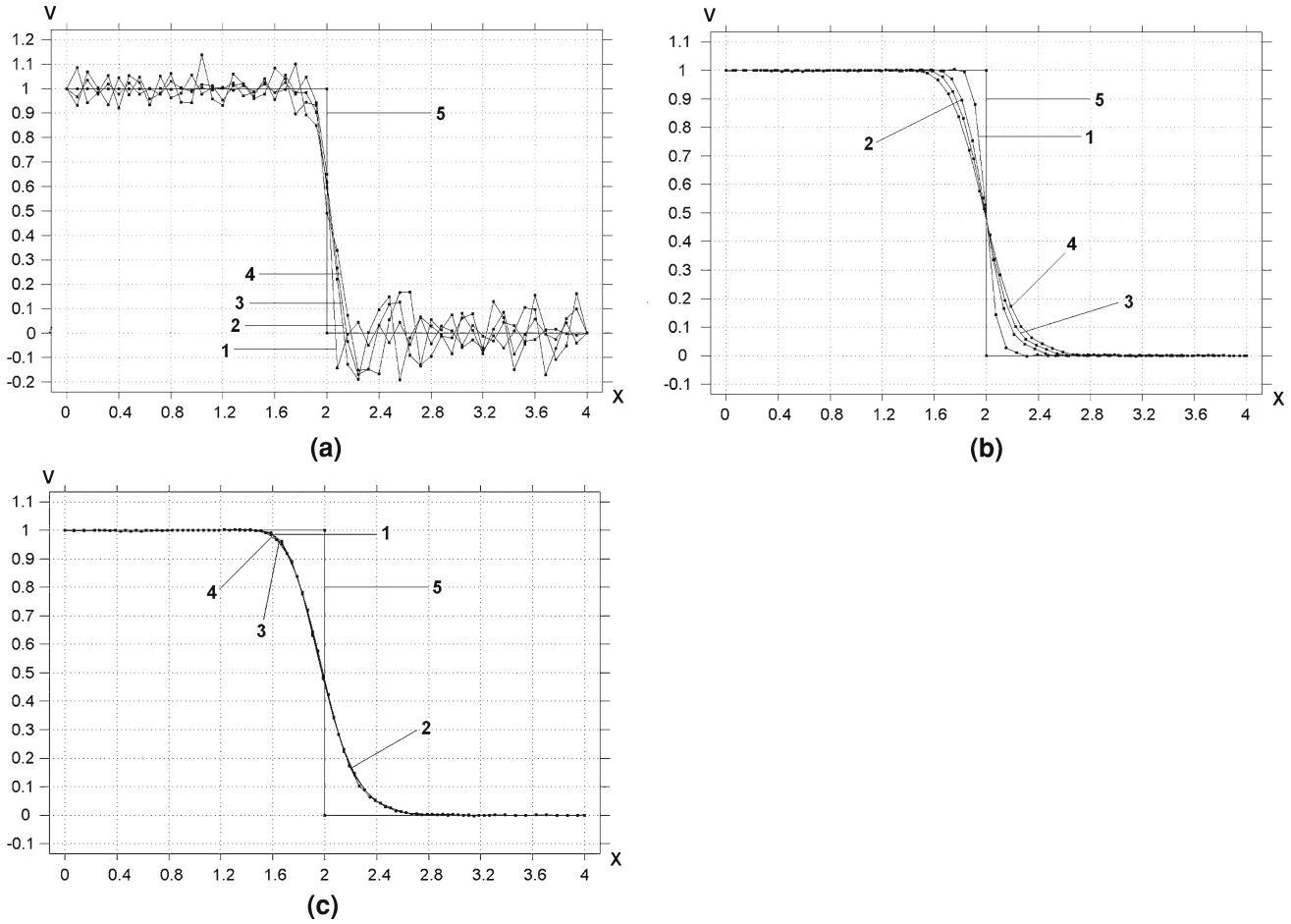

Fig. 5 Velocity distribution along the bar for long-term behavior calculated on a uniform mesh with 50 quadratic 3-node finite elements. **a**, **b**, **c** correspond to the solutions obtained by the trapezoidal rule, by the new strategy with post-processing based on uniform time increments of different sizes (using varying α) at different observation times, and by the new strategy with post-processing based on uniform time increments of the same sizes (using constant $\alpha = 1.13$) at different observation times; see the text for the explanations. Curves 1, 2, 3 and 4 correspond to the observation times $T = 2, 42, 98$ and 202, respectively. Curve 5 corresponds to the analytical solutions at the observation times $T = 2, 42, 98$ and 202

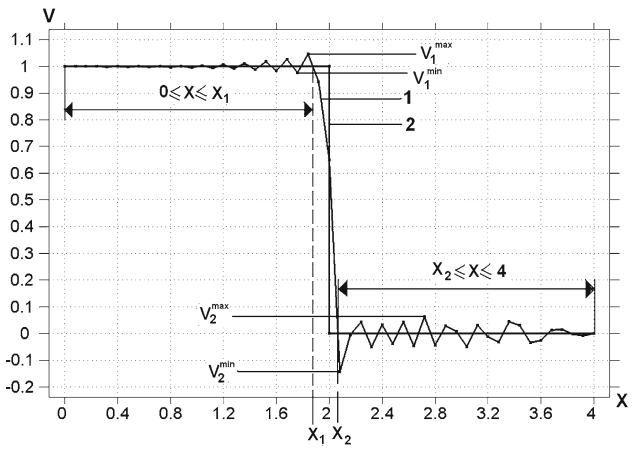

Fig. 6 The determination of the measure of spurious high-frequency oscillations from a numerical solution for the velocity (curve 1); see the text for explanations. Curve 2 corresponds to an analytical solution for the velocity

different observation times T for linear and quadratic elements. Then, by the use of Eq. 9, the coefficient α was recalculated for these observation times or, more precisely, for the corresponding parameters $N_1 = \frac{cT}{\Delta x}$. Finally, we found that the following formula

$$\alpha\left(\frac{cT}{\Delta x}\right) = a_1\left(\frac{cT}{\Delta x}\right)^{a_2}, \tag{10}$$

where $a_1 = 0.279$ and $a_2 = 0.3305$ for linear elements, and $a_1 = 0.1785$ and $a_2 = 0.2357$ for quadratic elements, yields a good approximation of the coefficient α for any value of parameter N_1; see Fig. 7.

Remark 1 The use of Eqs. 9 and 10 for different elastodynamics problems is based on the assumption that for different problems the range of spurious high-frequency oscillations depends on the size of finite elements Δx and the observation time T. For the 1D impact problem, all frequencies of

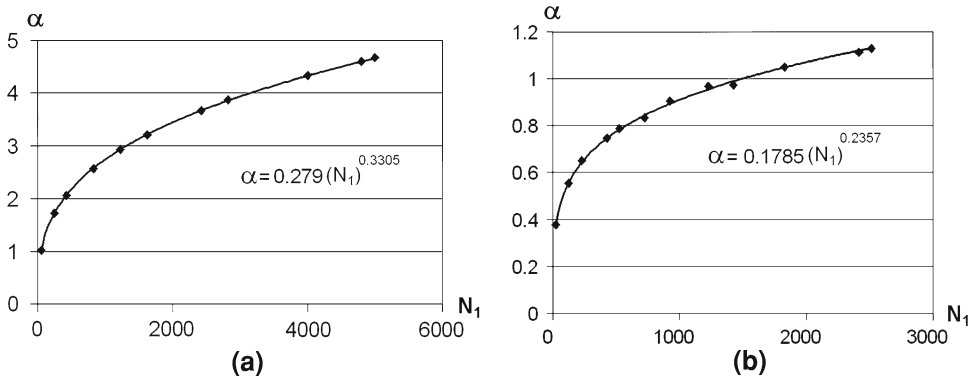

Fig. 7 The approximation of coefficient α as a function of parameter N_1 (see the text for explanations) for uniform meshes with linear **a** and quadratic **b** elements. ■—results from numerical experiments; ___—analytical approximation

a semi-discrete finite element model are excited. The numerical dissipation described by Eqs. 9 and 10 and calibrated for the 1D impact problem, determines (indirectly) and filters all spurious high-frequency oscillations for the given size of a finite element Δx and the given observation time T. For other elastodynamics problems, for which just some frequencies of a semi-discrete model are excited, the numerical dissipation described by Eqs. 9 and 10 filters the same range of high frequencies as that for the 1D impact problem. Our experience shows that non-oscillatory numerical results are obtained with Eqs. 9 and 10 for different elastodynamics problems; i.e., the assumption that the range of spurious oscillations depends on Δx and T, is valid.

Remark 2 At mesh refinement, Eqs. 9 and 10 yield a decreasing time increment at the same observation time. It means that at mesh refinement more modes of a semi-discrete system, Eq. 1, will be included in the solution after pre- or post-processing; i.e. a numerical solution will be more accurate at mesh refinement (similar to the modal decomposition method with an increasing number of modes).

As we mentioned before, for post-processing we used $N = 10$ time increments. Below we will explain the selection of this number $N = 10$ in calculations. Numerical experiments show that any number of time increments can be used for post-processing with the new first-order TCG method. Spurious oscillations can be filtered even with one time increment if a relatively large size of a time increment is used. Computation time for post-processing can be also reduced if a small number of time increments is used for post-processing. However, the accuracy of numerical results after post-processing depends on the number of time increments. The velocity distribution after post-processing with 2, 5, 10, 20 and 40 time increments is given in Figs. 8 and 9. Linear and quadratic finite elements as well as two different observation times are used in calculations. Numerical results show that Eq. (9) describes well the necessary amount of numerical dissipation for different selected numbers N of time increments used for post-processing; i.e., after post-processing the relative error is $e \approx 0.25\%$ for different N. Figures. 8 and 9 show that the accuracy of non-oscillatory solutions increases with the increase in the number N of time increments (i.e., the width of the wave front decreases). The results obtained with 10 time increments for post-processing are much more accurate than those obtained with 2 and 5 time increments; see curves 1, 2 and 3 in Figs. 8a, c and 9a, c. However, the difference in accuracy between the results after post-processing with 10, 20 and 40 is insignificant; see curves 1, 2 and 3 in Figs. 8b, d and 9b, d. Therefore we selected $N = 10$ as an optimal number with respect to computation time and accuracy.

Finally, we will show that the boundary conditions do not affect the necessary amount of numerical dissipation expressed by Eq. 9. In addition to the 1D impact problems for a bar with length $L = 4$, let us consider the 1D impact problem for a bar with length $L = 40$ with the same boundary and initial conditions as for the bar with $L = 4$. Uniform meshes with 1,000 linear and 500 quadratic elements are used for the long bar with $L = 40$ (i.e., the same sizes of finite elements are used for both bars). Figure 10 shows the comparison of the velocity distribution at observation time $T = 34$ for the two bars. For convenience of comparison, the analytical and numerical solutions for the long bar are shifted to the left along the x-axis by the value 32. In this case, the analytical solutions for the two bars coincide; see curve 3 in Fig. 10. The numerical solutions for the two bars after basic computations (see curves 1 and 2 in Fig. 10a and c) and after post-processing (see curves 1 and 2 in Fig. 10b and d) are slightly different. However, the same numerical dissipation is required for post-processing in order to obtain the same error e related to spurious oscillations.

3.1.3 Numerical results

The velocity distributions in Figs. 4a and 5a have a lot of spurious oscillations. Therefore, it is difficult to compare the accuracy of numerical results obtained on different meshes

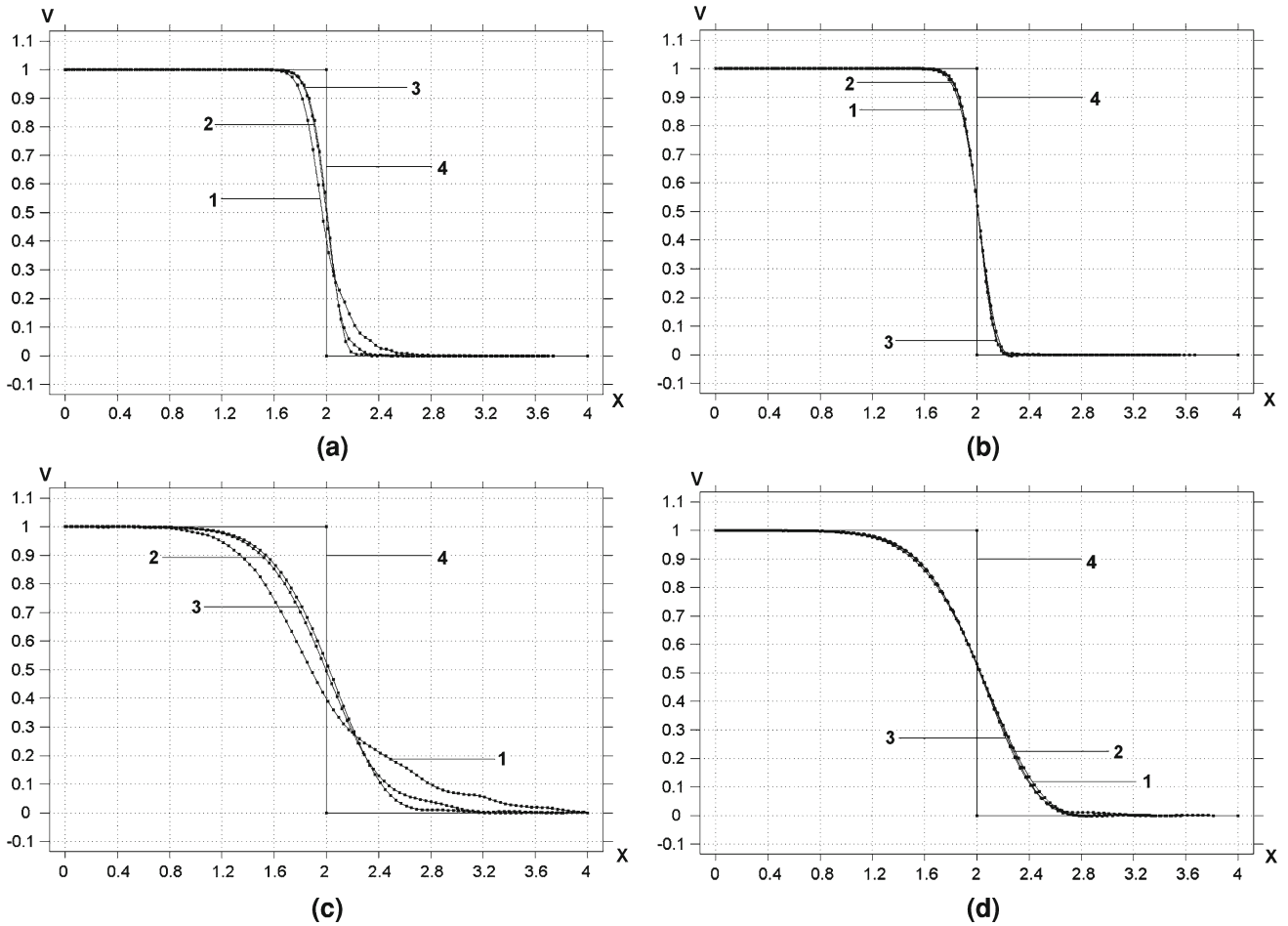

Fig. 8 Velocity distribution along the bar calculated on a uniform mesh with 100 linear 2-node finite elements at observation times $T = 2$ (**a, b**) and $T = 98$ (**c, d**). Curves 1, 2 and 3 in (**a, c**) correspond to the solutions obtained after post-processing with 2, 5 and 10 uniform time increments. Curves 1, 2 and 3 in (**b, d**) correspond to the solutions obtained after post-processing with 10, 20 and 40 time increments. Curve 4 corresponds to the analytical solutions at the observation times $T = 2$ and 98

and at different observation times (the selected observation times correspond to many reflections of the elastic wave from the ends of the bar). Below we discuss the numerical results obtained by the application of the new solution strategy combined with the first-order implicit TCG method with large numerical dissipation used for the filtering of spurious oscillations. As discussed above, $N = 10$ time increments are used for the filtering procedure with minimum necessary amount of numerical dissipation calculated according to Eqs. 9 and 10. As can be seen from Figs. 4b and 5b, non-oscillatory results are obtained for the impact problem at different observation times on uniform meshes with linear and quadratic elements. The following coefficients $\alpha = 1.02; 2.76; 3.66; 4.67$ (according to Eqs. 10) and the corresponding sizes of time increments $\Delta t = 0.0331;\ 0.08945; 0.11872; 0.15139$ (according to Eq. 9) are used for post-processing on the uniform mesh with 100 linear elements at the observation times $T = 2; 42; 98; 202$. The following coefficients $\alpha = 0.37; 0.78; 0.95; 1.13$ (according to Eq. (10)) and the corresponding sizes of time increments $\Delta t = 0.02397; 0.05048; 0.06172; 0.07324$ (according to Eq. 9) are used for post-processing on the uniform mesh with 50 quadratic elements at the observation times $T = 2; 42; 98; 202$. As we can expect, the numerical results at greater observation times are less accurate due to the accumulation of the dispersion error of the finite element solution with the increase in observation time. We also solve the impact problem using post-processing with the equally large numerical dissipation (related to the maximum selected observation time $T = 202$) for all selected observation times; i.e., the coefficient $\alpha = 4.67$ and the time increment $\Delta t = 0.15139$ as well as the coefficient $\alpha = 1.13$ and the time increment $\Delta t = 0.07324$ are used in Figs. 4c and 5c for all observation times for linear and quadratic elements, respectively. In this case the accuracy of numerical results is approximately the same at all observation times; i.e., non-oscillatory results with practically the same slope of the

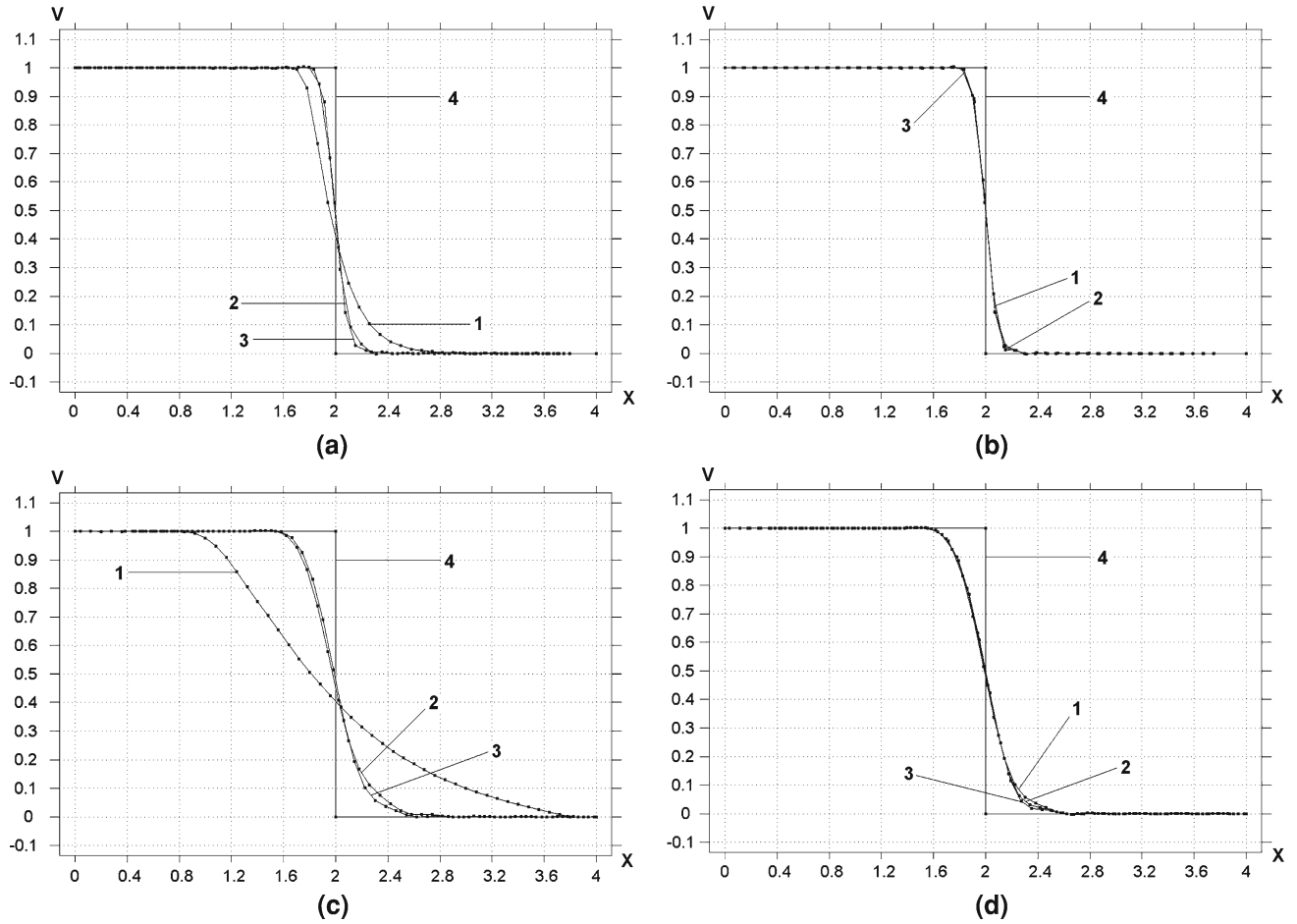

Fig. 9 Velocity distribution along the bar calculated on a uniform mesh with 50 quadratic 3-node finite elements at observation times $T = 2$ (**a, b**) and $T = 98$ (**c, d**). Curves 1, 2 and 3 in (**a, c**) correspond to the solutions obtained after post-processing with 2, 5 and 10 uniform time increments. Curves 1, 2 and 3 in (**b, d**) correspond to the solutions obtained after post-processing with 10, 20 and 40 time increments. Curve 4 corresponds to the analytical solutions at the observation times $T = 2$ and 98

wave front are obtained. However, if the minimum necessary amount of numerical dissipation is used, the results are more accurate (see curves 1,2,3 in Fig. 4b, c for linear elements and curves 1,2,3 in Fig. 5b, c for quadratic elements).

Next, for the comparison of the effectiveness of linear and quadratic elements for wave propagation problems, we simultaneously plot the velocity distribution along the x-axis (shown in Figs. 4b and 5b) for linear and quadratic elements at different observation times; see Fig. 11. We remind that the uniform meshes with linear and quadratic elements have the same number of degrees of freedom. As can be seen from Fig. 11, quadratic elements yield much better accuracy, especially with the increase in observation time.

The instantaneous application of the finite velocity $v_0 = 1$ at the left end of the bar excites a high-frequency response of the bar at the initial time only. Therefore, according to the new solution strategy, pre-processing or post-processing can be applied to this problem for filtering spurious oscillations; see [13]. Numerical results show that practically the same velocity distribution as shown in Figs. 4b and 5b are obtained if pre-processing instead of post-processing (with the same sizes of time increments as for post-processing) are used. Figures 12 and 13 also show the variation of velocity with time in the middle of the bar ($x = 2$) after basic computations (a) and using the new approach (pre-processing plus basic computations) with linear and quadratic elements. For pre-processing the size of time increment is calculated from Eqs. (9) and (10) for the selected observation time $T = 100$ and equals $\Delta t = 0.12$ and $\Delta t = 0.06211$ for linear and quadratic elements, respectively. As can be seen, the variation of the velocity in time in the middle of the bar after basic computations contains a lot of spurious oscillations which make the solutions impracticable; see Figs. 12a and 13a. The new strategy filters the spurious oscillations and yields the accurate and non-oscillatory results; see Figs. 12b, c and 13b, c. The same as for the spatial distribution, the time variation of

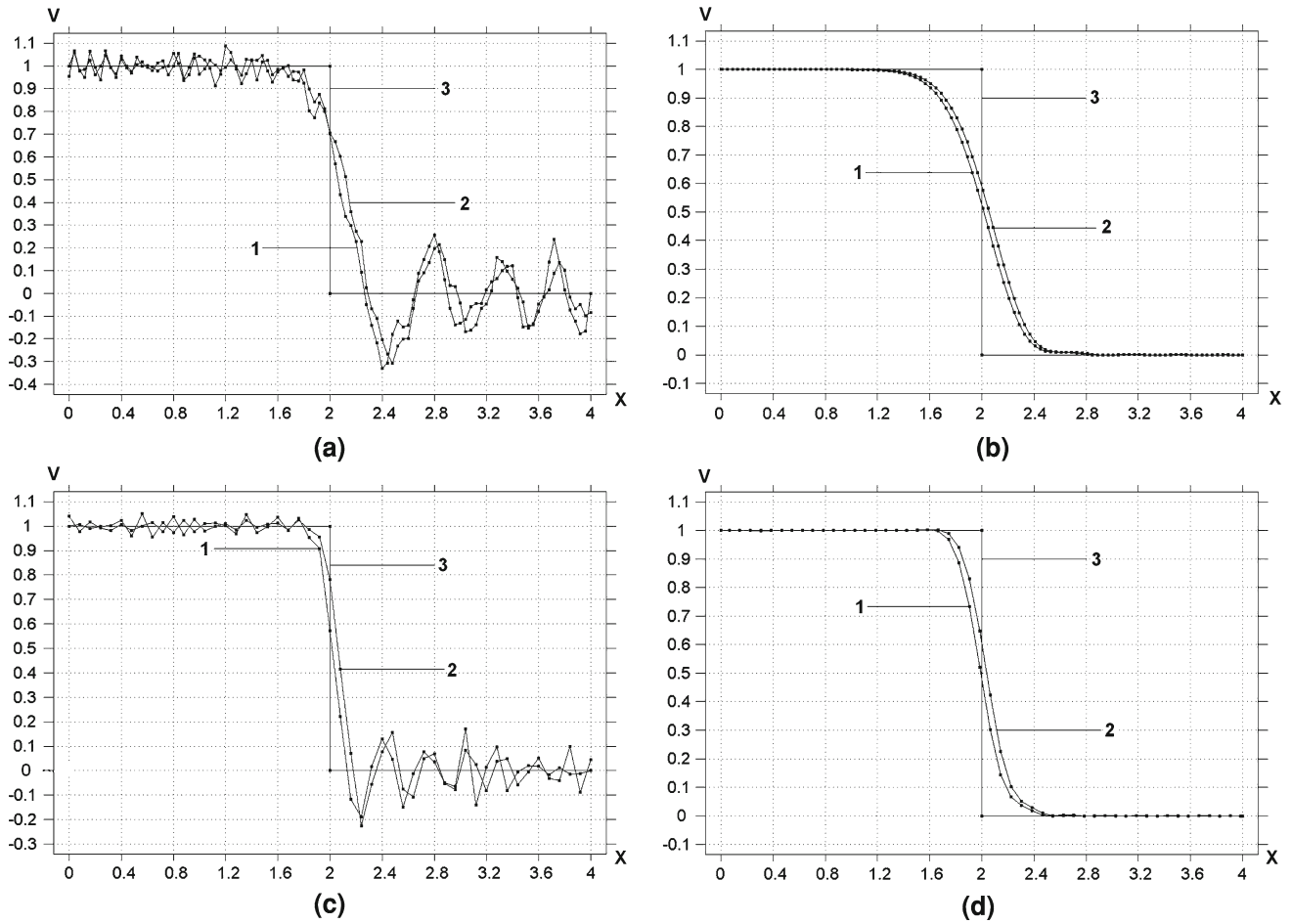

Fig. 10 Velocity distribution along the bar for two bars of length $L = 4$ (curves 1) and $L = 40$ (curves 2) at the observation time $T = 34$; see the text for explanations. **a**, **c** and **b**, **d** correspond to the solutions obtained by the trapezoidal rule and by the new strategy with post-processing based on 10 uniform time increments, respectively; $\alpha = 2.57$ and $\alpha = 0.76$ are used for linear and quadratic elements, respectively. Uniform meshes with 100 (for $L = 4$) and 1,000 (for $L = 40$) linear elements and 50 (for $L = 4$) and 500 (for $L = 40$) quadratic elements are used. Curve 3 is the analytical solution at observation time $T = 34$

the velocity is much more accurate for quadratic elements than for linear elements, see Fig. 14.

3.2 Impact of an elastic cylinder against a rigid wall (the axisymmetric formulation)

The next problem is a more general axisymmetric formulation of the 1D impact problem considered above; see Fig. 15. A cylinder of length $L = 2.5$ and radius $R = 1$ is considered. The z-axis is the axis of revolution. Young's modulus is chosen to be $E = 1$, Poisson's ratio to be $\nu = 0.3$, and the density to be $\rho = 1$. The following boundary conditions are applied: along boundary AB, $u_n = t$ (which corresponds to velocity $v_n = v_0 = 1$) and $\tau_n = 0$; along boundaries CD and AD, $\sigma_n = 0$ and $\tau_n = 0$; along boundary BC, $u_n = 0$ and $\tau_n = 0$, where u_n, v_n, and σ_n are the normal displacements, velocities and tractive forces, respectively; and τ_n are the tangential tractive forces. Initial displacements and velocities are zero; i.e., $u(r, z, 0) = v(r, z, 0) = 0$. To simplify the comparison of a numerical solution of the problem with the approximation of the analytical solution derived in [21] by means of the Laplace transform, the following dimensionless coordinates ($\bar{r}$ and $\bar{z}$), the dimensionless time $\bar{t}$

$$\bar{r} = \frac{r}{R}, \quad \bar{z} = \frac{z}{L}, \quad \bar{t} = \frac{tc_1}{R}, \tag{11}$$

and the normalized displacements $\bar{u}_i$, velocities $\bar{v}_i$, stresses $\bar{\sigma}_{ij}$ and strains $\bar{\varepsilon}_{ij}$

$$\bar{u}_i = \frac{u_i c_1}{R v_0}, \quad \bar{v}_i = \frac{v_i}{v_0}, \quad \bar{\varepsilon}_{ij} = \frac{\varepsilon_{ij} c_1}{v_0},$$
$$\bar{\sigma}_{ij} = \frac{\sigma_{ij} c_1 (1+\nu)(1-2\nu)}{\nu E v_0}, \quad i, j = r, z \tag{12}$$

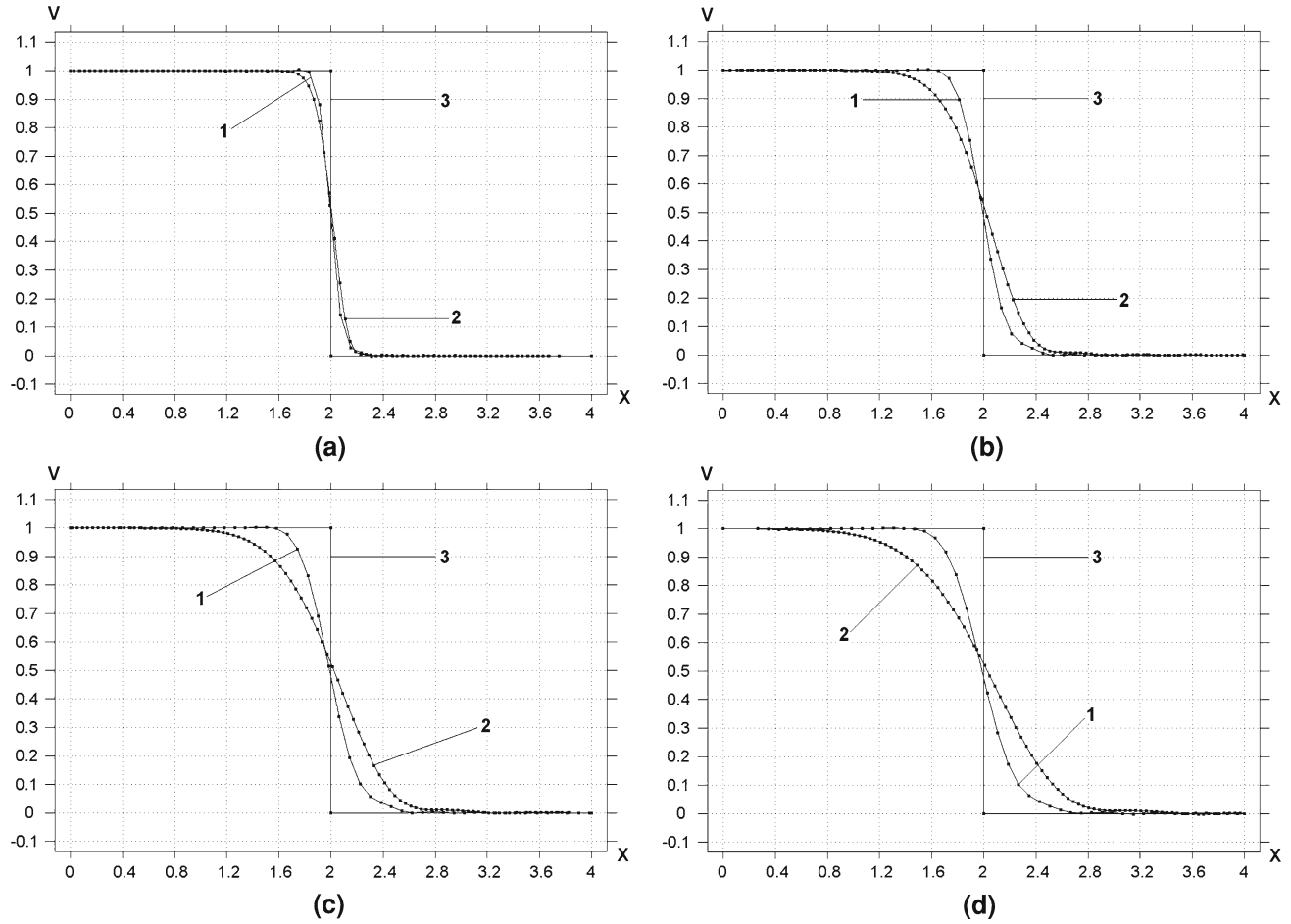

Fig. 11 Velocity distribution along the bar calculated on uniform meshes with 50 quadratic 3-node (curves 1) and with 100 linear 2-node (curves 2) finite elements. **a**, **b**, **c** and **d** correspond to the solutions obtained at observation times $T = 2, 42, 98$ and 202 using the new strategy with post-processing (see Figs. 4b and 5b). Curves 3 correspond to the analytical solutions at the observation times $T = 2, 42, 98$ and 202

are used, where $c_1 = \sqrt{\frac{E(1-\nu)}{2\rho(1+\nu)(1-2\nu)}}$ is the longitudinal wave rate. The dimensionless observation time is chosen to be $\bar{T} = 2$. The problem was solved on uniform meshes with 9-node quadratic quadrilateral elements, 6-node quadratic triangular elements and 4-node linear quadrilateral elements. A consistent mass matrix was used in all calculations. The trapezoidal rule with uniform time increments $\Delta\bar{t} = 0.00048$ was applied for basic computations. At these small time increments, the error in time was small and could be neglected. As in the previous 1D problem, the numerical results include many spurious high-frequency oscillations in stresses and velocities on the coarse and fine uniform meshes with 9-node quadratic quadrilateral elements after basic computations; see curves 1 in Fig. 16. These oscillations spoil the numerical solution and make it impractical. Thus, in order to filter the oscillations, post-processing using 10 uniform time increments with the implicit first-order TCG method is applied. For the selection of the minimum amount of numerical dissipation necessary for the considered axisymmetric problem, the following modification of Eq. 9 for multi-dimensional problems suggested in [13] is used

$$\begin{aligned}\Delta t &= \left[\max_{i,j}\ \alpha\left(\frac{c_i T}{\Delta x_j}\right)\right]\frac{\max\limits_j(\Delta x_j)}{\min\limits_i(c_i)}\Omega_{0.1}(N)\\ &= a_1\left[\frac{\max\limits_i(c_i)T}{\min\limits_j(\Delta x_j)}\right]^{a_2}\frac{\max\limits_j(\Delta x_j)}{\min\limits_i(c_i)}\Omega_{0.1}(N)\,,\end{aligned}\tag{13}$$

where $\max_i(c_i) = \max(c_1, c_2)$ and $\min_i(c_i) = \min(c_1, c_2)$ $(i = 1, 2)$ are the maximum and minimum values between the velocities of the longitudinal wave c_1 and the transversal wave $c_2 = \sqrt{\frac{E}{2\rho(1+\nu)}}$, Δx_j are the dimensions of finite elements along the axes x_j $(i = 1, 2$ for the 2D problems and $i = 1, 2, 3$ for the 3D problems). For uniform meshes with linear and quadratic quadrilateral elements in the case of multi-dimensional problems, we use the coefficients a_1 and a_2 obtained for the 1D case; see Eq. 10.

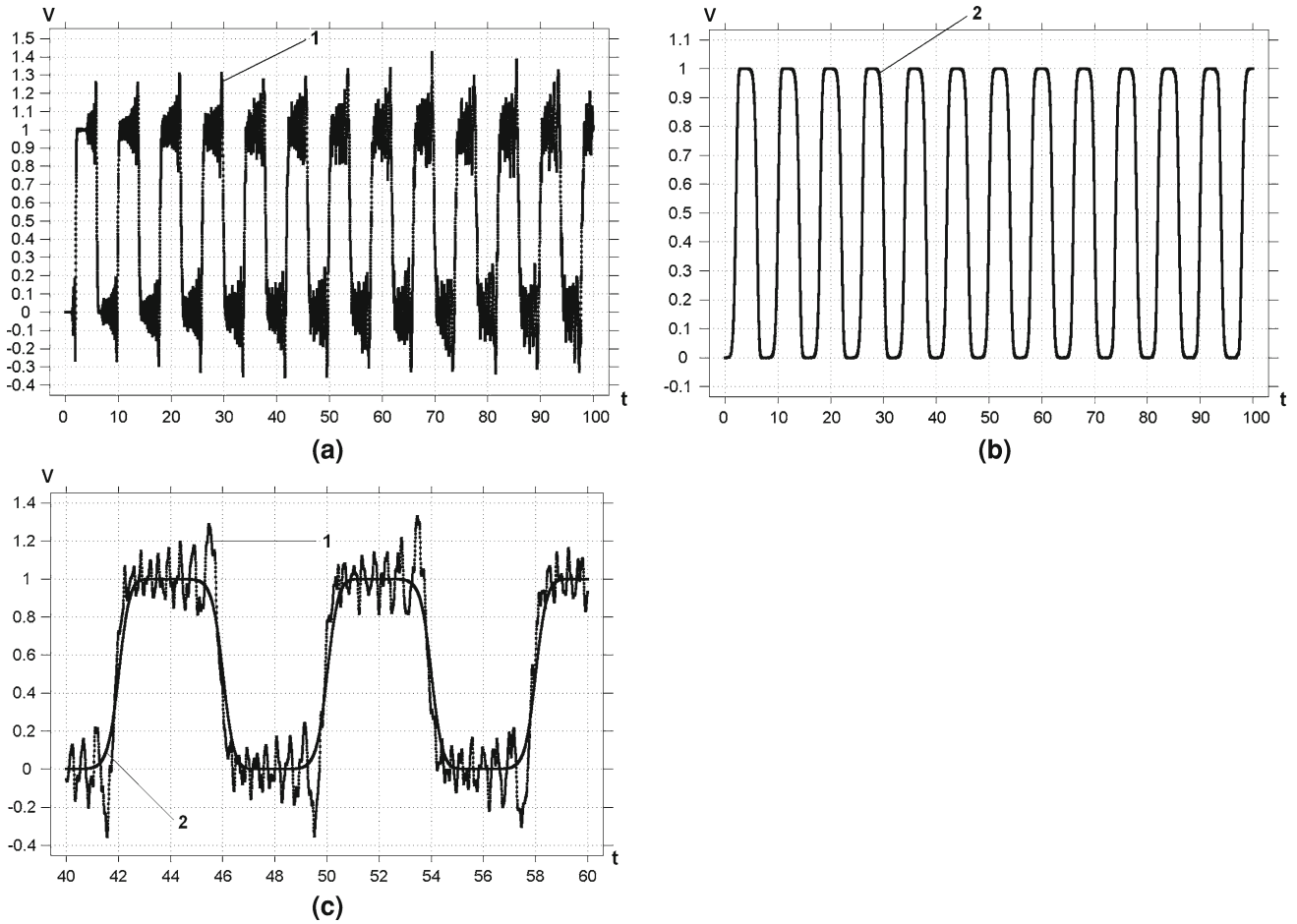

Fig. 12 The variation of the velocity in time in the middle of the bar ($X = 2$) calculated on a uniform mesh with 100 linear elements. **a** and **b** correspond to the solutions obtained by the trapezoidal rule and by the new solution strategy with pre-processing based on 10 uniform time increments. **c** shows curves 1(a) and 2(b) in the time interval $40 \leq t \leq 60$

Numerical results show that non-oscillatory smooth numerical solutions on uniform meshes with quadrilateral elements are obtained after post-processing based on the first-order TCG method with time increments calculated from Eqs. (10) and (13); see curves 2 in Fig. 16.

Figure 17 shows the convergence of non-oscillatory numerical results, obtained with the new solution strategy (basic computations plus post-processing) at mesh refinement, to the approximation of the analytical solution derived in [21] using the Laplace transform. Uniform meshes with $50 \times 100 = 5{,}000$, $100 \times 200 = 20{,}000$ and $200 \times 400 = 80{,}000$ quadrilateral 9 node quadratic elements were used. The approximate analytical solution (curves 1 in Fig. 17) has spurious oscillations due to Gibbs phenomena. The oscillations can clearly be seen for the range $2 < z/R < 2.5$ in Fig. 17 where the exact stresses and velocities are zero (a non-disturbed domain).

The instantaneous application of the finite velocity $v_0 = 1$ at the left end of the cylinder excites a high-frequency response of the cylinder at the initial time only (as in the previous 1D problem). Therefore, according to the new solution strategy, pre-processing or post-processing can be used for this problem for filtering spurious oscillations; see [13]. Numerical experiments show that the application of another scenario of the new solution strategy (pre-processing plus basic computations) to this problem yields non-oscillatory results close to those shown in Fig. 17 (the implicit first-order TCG method with 10 time increments is used for pre-processing with the same size of time increments as that used for post-processing). We should mention that from the computational point of view, pre-processing is more effective than post-processing if the variation of any parameter (velocity, stress or other parameter) in time at a specific point should be analyzed. Figure 18 shows the variation of the dimensionless velocity $\bar{v}_z$ in time in the middle of the axis of revolution (a, b) and in the middle of the external surface (c, d) after basic computations (a, c) and after pre-processing plus basic computations (b, d). As can be expected, there are a lot of

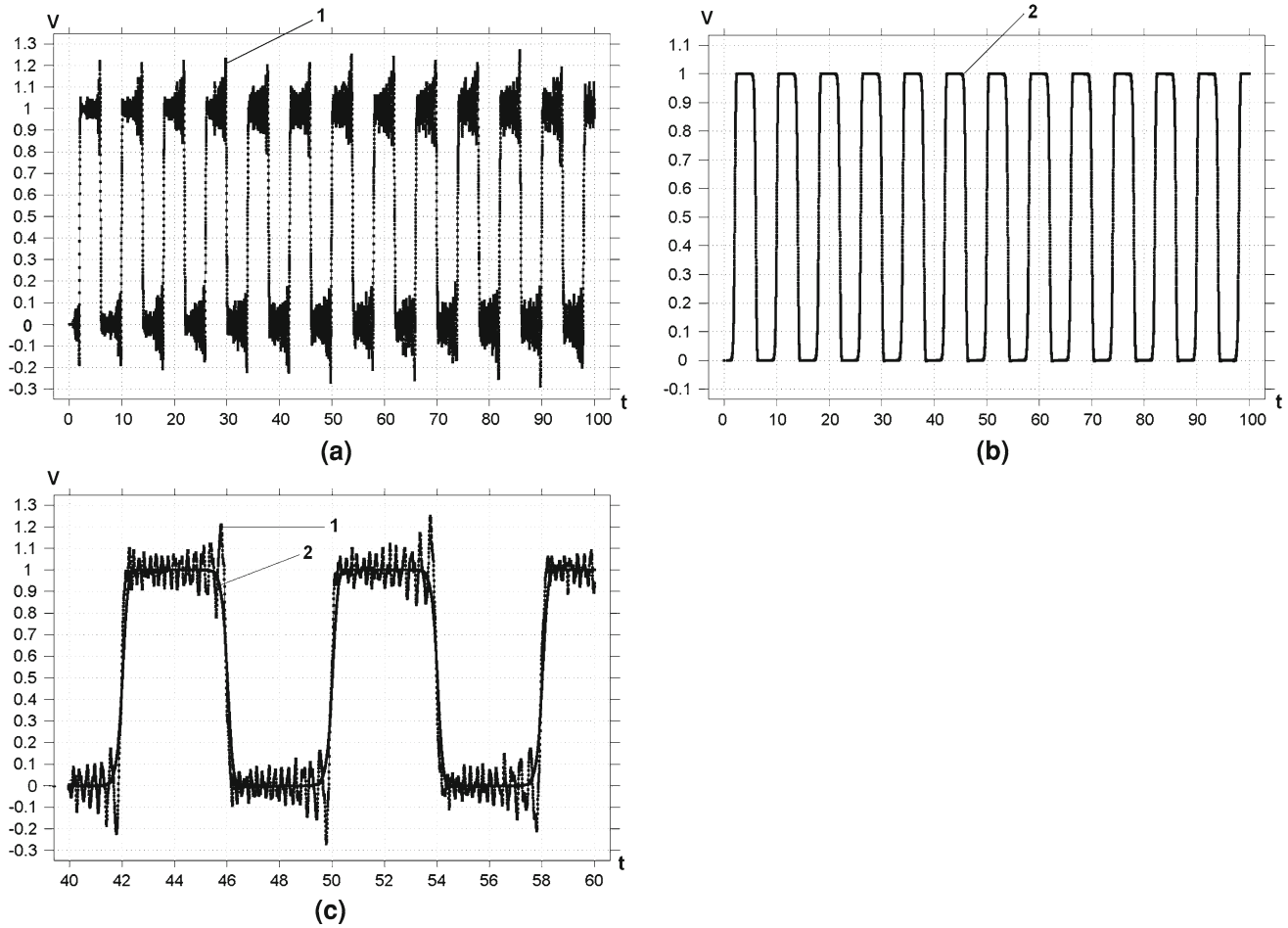

Fig. 13 The variation of the velocity in time in the middle of the bar ($X = 2$) calculated on a uniform mesh with 50 quadratic elements. **a** and **b** correspond to the solutions obtained by the trapezoidal rule and by the new solution strategy with pre-processing based on 10 uniform time increments. **c** shows curves 1(a) and 2(b) in the time interval $40 \leq t \leq 60$

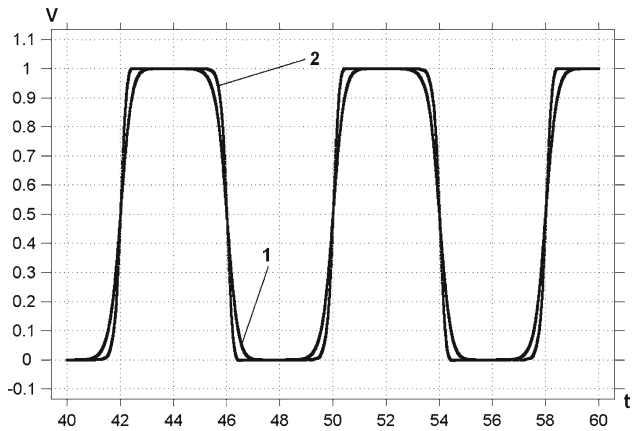

Fig. 14 The comparison of the curves from Figs. 12b and 13b related to linear (curve 1) and quadratic (curve 2) elements in the time interval $40 \leq t \leq 60$

spurious oscillations after basic computations, especially at the point on the axis of revolution. The new technique with pre-processing yields non-oscillatory accurate results at these points; see Fig. 18b, d.

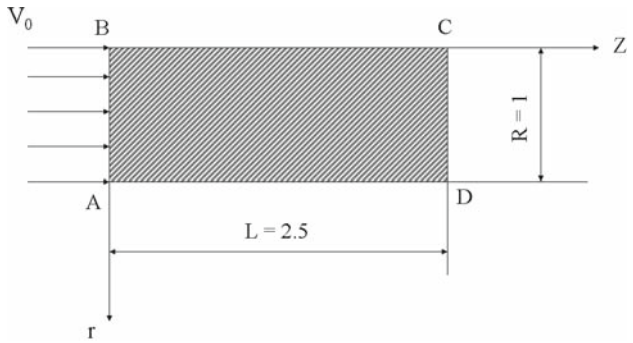

Fig. 15 Axisymmetric impact of an elastic cylinder of length L and radius R against a rigid wall. z is the axis of revolution

Next, we will compare the effectiveness of linear and quadratic elements for the considered axisymmetric problem. The problem is computed using the new technique on a mesh with $400 \times 800 = 320{,}000$ quadrilateral 4 node linear elements and a mesh with $200 \times 400 = 80{,}000$ quadrilateral 9 node quadratic elements. The meshes have the same number

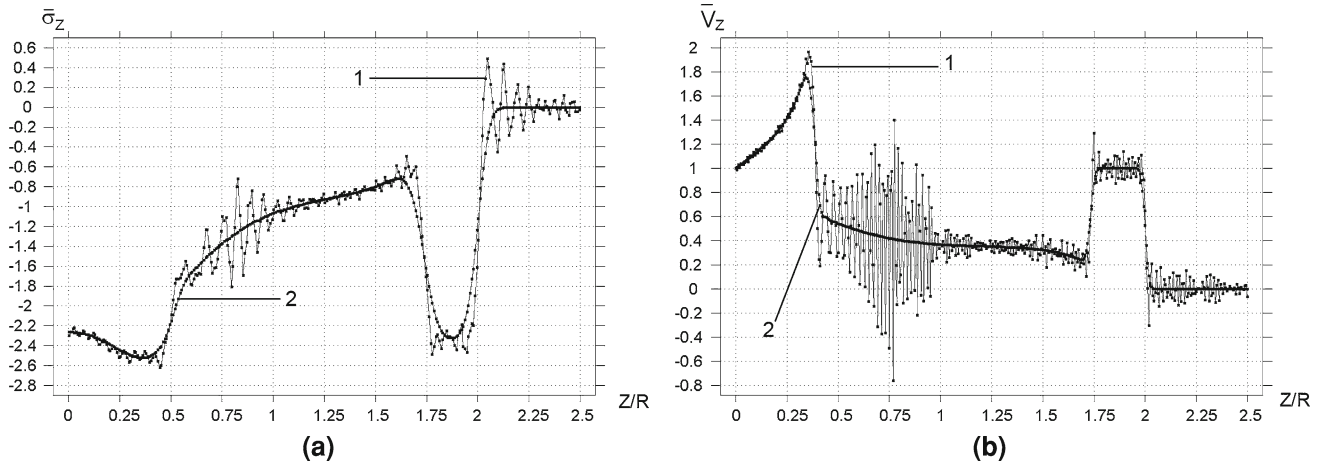

Fig. 16 The distribution of the dimensionless axial stress $\bar{\sigma}_z$ (**a**) and dimensionless velocity $\bar{v}_z$ (**b**) along the dimensionless axial coordinate $\bar{z} = z/R$ and the fixed dimensionless radial coordinate $\bar{r}$ ($\bar{r} = 0.05$ for (**a**) and $\bar{r} = 0$ for (**b**)) at dimensionless time $\bar{T} = c_1 t/R = 2$. Curves 1 and 2 correspond to the numerical solutions obtained by the trapezoidal rule and by the new solution strategy, respectively. Uniform meshes with 5,000 (**a**) and 80,000 (**b**) quadratic $Q9$ elements are used

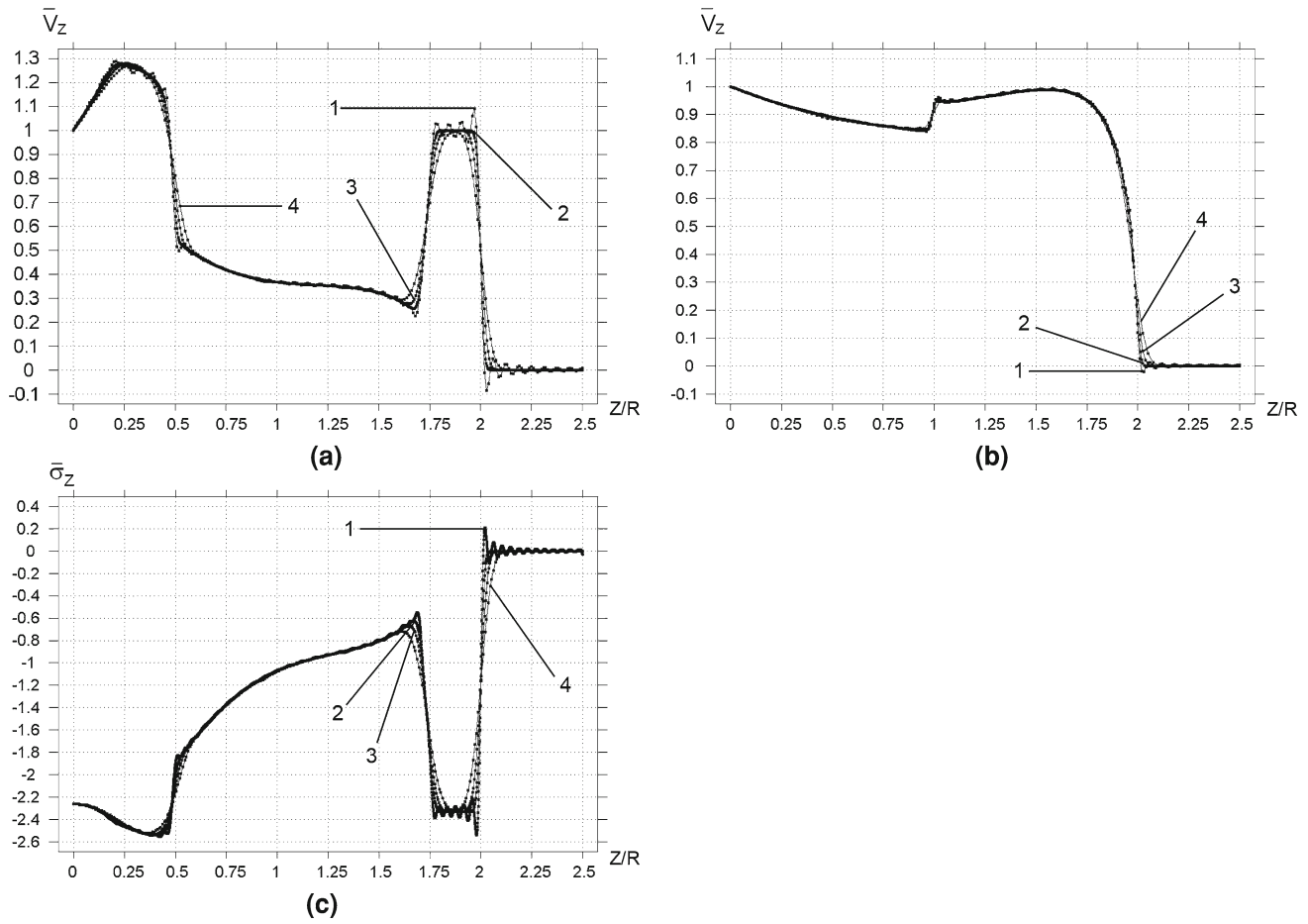

Fig. 17 The distribution of the dimensionless velocity $\bar{v}_z$ (**a, b**) and axial stress $\bar{\sigma}_z$ **c** along the dimensionless axial coordinate $\bar{z} = z/R$ and the fixed dimensionless radial coordinate $\bar{r}$ ($\bar{r} = 0.05$ for **a c**, and $\bar{r} = 1$ for **b**) at dimensionless time $\bar{T} = c_1 t/R = 2$. Curve 1 is the approximation of the analytical solution; see [21]. Curves 2, 3 and 4 correspond to the numerical solutions obtained with the new solution strategy on uniform meshes with 80,000, 20,000, and 5,000 quadratic $Q9$ elements, respectively

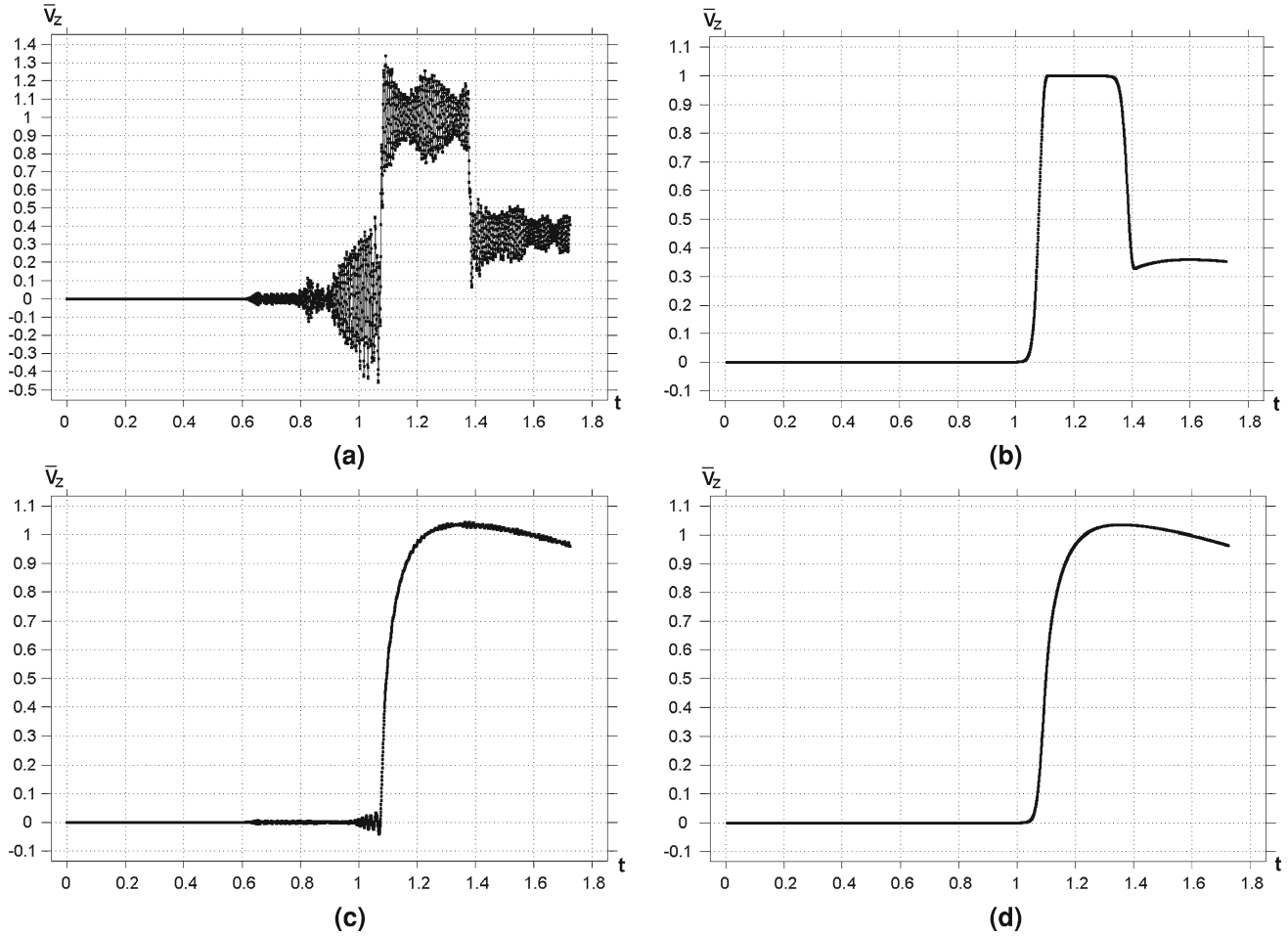

Fig. 18 The variation of the dimensionless velocity $\bar{v}_z$ in time in the middle of the cylinder on the axis of revolution (**a, b**) and on the external surface (**c, d**) calculated on a uniform mesh with 80000 quadratic Q9 elements. **a**, **c** and **b**, **d** correspond to the numerical results obtained by the trapezoidal rule and by the new solution strategy with pre-processing, respectively

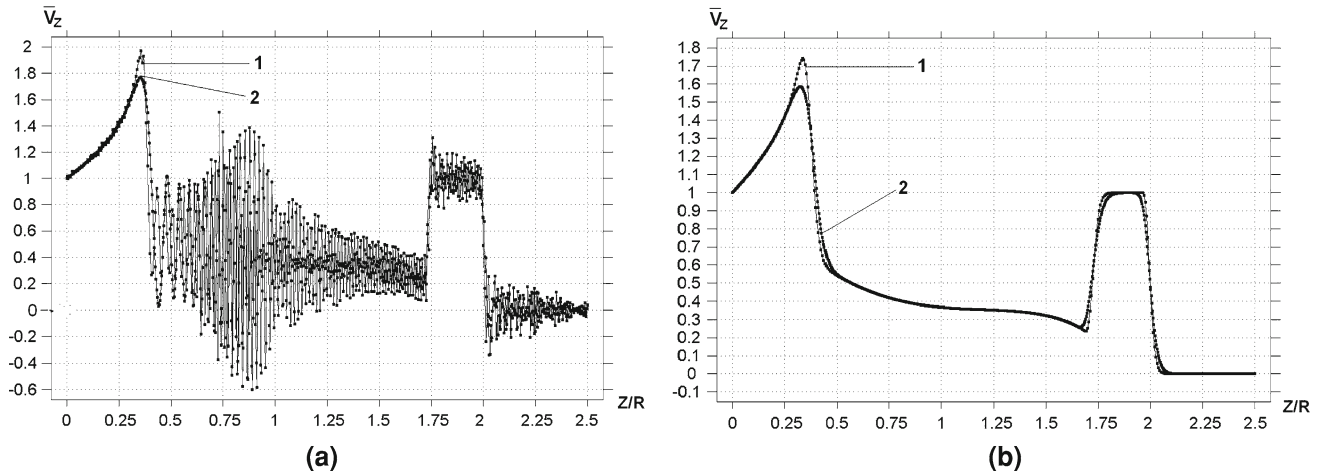

Fig. 19 The distribution of the dimensionless velocity $\bar{v}_z$ along the axis of revolution ($\bar{r} = 0$) at dimensionless time $\bar{T} = c_1 t/R = 2$, obtained by the trapezoidal rule **a** and by the new solution strategy with post-processing **b** on the uniform meshes with 320,000 linear 4-node elements (curves 2) and 80,000 quadratic 9-node elements (curves 1)

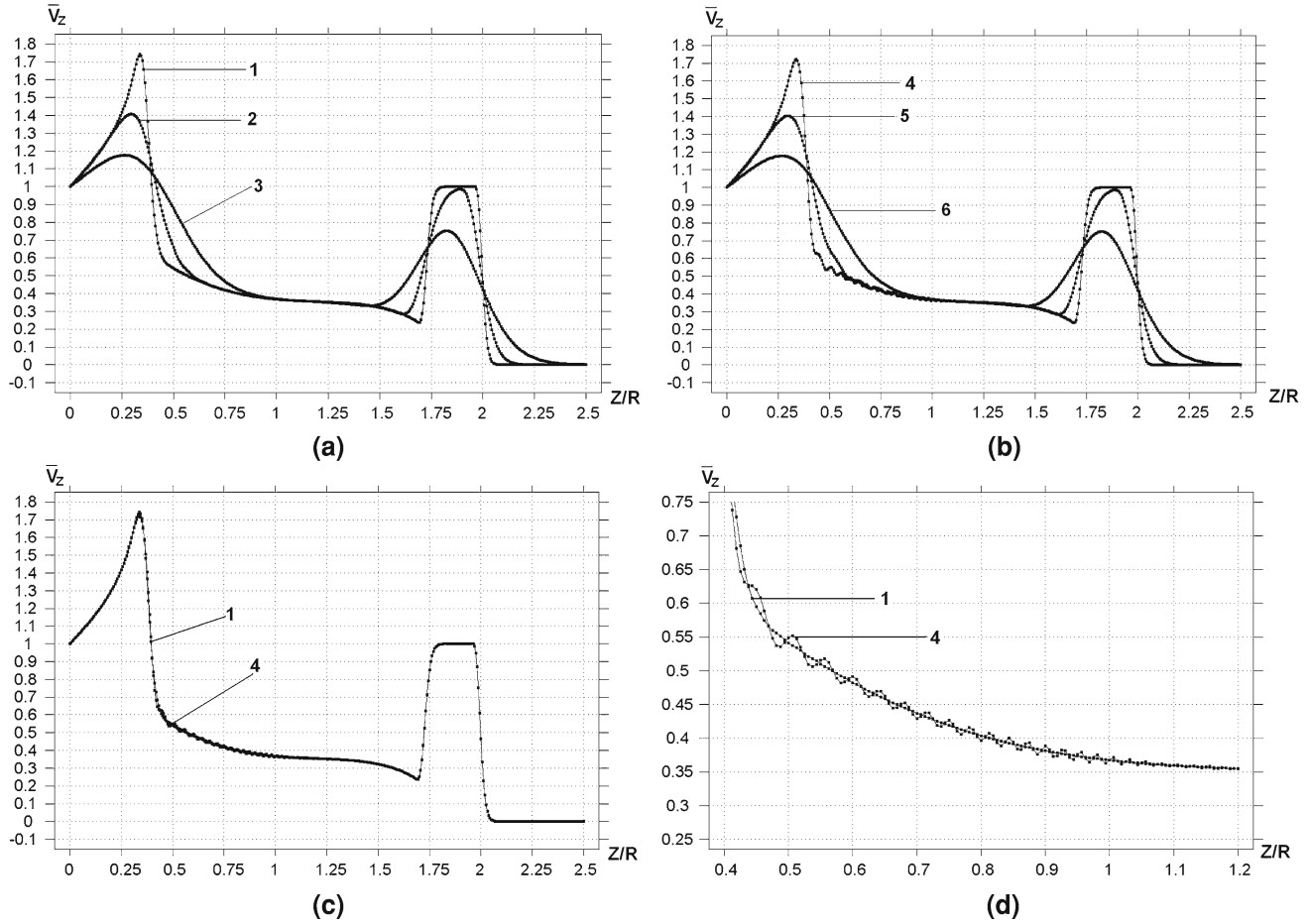

Fig. 20 The distribution of the dimensionless velocity $\bar{v}_z$ along the axis of revolution ($\bar{r} = 0$) at dimensionless time $\bar{T} = c_1 t/R = 2$ calculated by the new solution strategy on uniform meshes with 80,000 (**a**, curve 1), 20,000 (**a**, curve 2), 8,000 (**a**, curve 3) quadrilateral elements and 160,000 (**b**, curve 4), 40,000 (**b**, curve 5), 16,000 (**b**, curve 6) triangular elements. **c** and **d** show the comparison of curves 1 and 4 in the intervals $0 \le z/R \le 2.5$ **c** and $0.4 \le z/R \le 1.2$ **d**

642,402 of degrees of freedom. The velocity distributions along the axis of revolution after basic computations and after basic computations plus post-processing are shown in Fig. 19. As in the previous 1D problems, the quadratic elements yield better accuracy than linear elements for multi-dimensional wave propagation problems at the same numbers of degrees of freedom.

Finally, we will study the application of the new strategy (basic computations plus post-processing) and formulas for the necessary amount of numerical dissipation, Eqs. 10 and 13, to the solution of wave propagation problems on uniform meshes with quadrilateral and triangular elements having different aspect ratios (or using mesh refinement in one direction). We will use three uniform meshes with $200 \times 400 = 80{,}000$, $50 \times 400 = 20{,}000$ and $20 \times 400 = 8{,}000$ quadrilateral 9-node quadratic elements (where 400 elements is used along the axis of revolution) and three uniform meshes with triangular 6-node quadratic elements. The triangular meshes are obtained by the division of each 9-node rectangular element of the uniform meshes with quadrilateral elements into two 6-node triangular elements; i.e., the corresponding meshes with 9-node rectangular elements and 6-node triangular elements have the same number of degrees of freedom. The distribution of dimensionless axial velocity along the axis of revolution calculated on all six meshes is shown in Fig. 20. As we can see, the new technique with the minimum necessary amount of numerical dissipation calculated from Eqs. 10 and 13 yields non-oscillatory results for all aspect ratios of quadrilateral finite elements. However, numerical results on the triangular meshes contain small oscillations; see Fig. 20b, c and d. It means that additional numerical dissipation (the modification of Eqs. (10) and (13)) for these triangular elements should be given. We also should mention that at the same number of degrees of freedom, numerical results on meshes with quadrilateral elements are slightly more accurate than those containing small spurious oscillations on the corresponding meshes with triangular elements; see Fig. 20c, d.

4 Concluding remarks

The new numerical approach based on the new solution strategy and the new-time integration methods for the first time yields accurate and non-oscillatory solutions for wave propagation in elastic materials. A new analytical expression for the minimum necessary amount of numerical dissipation used by the new implicit time-integration method for filtering spurious oscillations is suggested. It is shown that the new approach with the new analytical formula for numerical dissipation yields accurate and non-oscillatory results for 1D and 2D wave propagation problems on uniform meshes with quadrilateral finite elements. In contrast to existing approaches, the new technique does not require any guesswork for the selection of artificial viscosity and does not require interaction between users and computer codes for the suppression of spurious high-frequency oscillations. Further study is needed for the determination of the minimum necessary amount of numerical dissipation for the new technique applied on non-uniform meshes and for non-homogeneous materials. In this case, new parameters describing the space variation of material properties and the dimension variation of finite elements for non-uniform meshes should be included in the expression for the amount of numerical dissipation. We would like to mention that the new technique with the new explicit time-integration methods (see [13]) also yields accurate and non-oscillatory results for wave propagation problems. However, the selection of analytical expressions for the minimum necessary amount of numerical dissipation for the explicit methods requires additional study and will be considered elsewhere.

Acknowledgments The research has been supported in part by the Texas Higher Education Coordinating Board under grant 003644 0008 2006.

References

1. Bathe KJ (1996) Finite element procedures. Prentice-Hall, Upper Saddle River
2. Benson DJ (1992) Computational methods in Lagrangian and Eulerian hydrocodes. Comput Methods Appl Mech Eng 99(2–3): 235–394
3. Chien CC, Wu TY (2000) Improved predictor/multi-corrector algorithm for a time-discontinuous galerkin finite element method in structural dynamics. Comput Mech 25(5):430–437
4. Govoni L, Mancuso M, Ubertini F (2006) Hierarchical higher-order dissipative methods for transient analysis. Int J Numer Methods Eng 67(12):1730–1767
5. Hilber HM, Hughes TJR (1978) Collocation, dissipation and 'overshoot' for time integration schemes in structural dynamics. Earthquake Eng Struct Dyn 6(1):99–117
6. Hilber HM, Hughes TJR, Taylor RL (1977) Improved numerical dissipation for time integration algorithms in structural dynamics. Earthquake Eng Struct Dyn 5(3):283–292
7. Houbolt JC (1950) A recurrence matrix solution for the dynamic response of elastic aircraft. J Aeronaut Sci 17:540–550
8. Hughes TJR (1987) The finite element method: linear static and dynamic finite element analysis. Prentice- Hall, Englewood Cliffs
9. Hulbert GM (1992) Discontinuity-capturing operators for elastodynamics. Comput Methods Appl Mech Eng 96(3):409–426
10. Hulbert GM, Hughes TJR (1990) Space-time finite element methods for second-order hyperbolic equations. Comput Methods Appl Mech Eng 84(3):327–348
11. Idesman AV (2007) A new high-order accurate continuous galerkin method for linear elastodynamics problems. Comput Mech 40:261–279
12. Idesman AV (2007) Solution of linear elastodynamics problems with space-time finite elements on structured and unstructured meshes. Comput Methods Appl Mech Eng 196:1787–1815
13. Idesman AV (2008) A new solution strategy and a new look at time-integration methods for elastodynamics. Comput Methods Appl Mech Eng 1–59 (submitted)
14. Jiang L, Rogers RJ (1990) Effects of spatial discretization on dispersion and spurious oscillations in elastic wave propagation. Int J Numer Methods Eng 29(6):1205–1218
15. Krenk S (2001) Dispersion-corrected explicit integration of the wave equation. Comput Methods Appl Mech Eng 191:975–987
16. Krenk S (2006) State-space time integration with energy control and fourth-order accuracy for linear dynamic systems. Int J Numer Methods Eng 65(5):595–619
17. Kunthong P, Thompson LL (2005) An efficient solver for the high-order accurate time-discontinuous Galerkin (tdg) method for second-order hyperbolic systems. Finite Elements Anal Design 41(7-8):729–762
18. Mancuso M, Ubertini F (2003) An efficient integration procedure for linear dynamics based on a time discontinuous Galerkin formulation. Comput Mech 32(3):154–168
19. Newmark NM (1959) A method of computation for structural dynamics. J Eng Mech Div ASCE 85(EM 3):67–94
20. Park KC (1975) Evaluating time integration methods for nonlinear dynamic analysis. In: Belytschko T et al (eds) Finite element analysis of transient nonlinear behavior. AMD 14, ASME, New York, pp 35–58
21. Vales F, Moravka S, Brepta R, Cerv J (1996) Wave propagation in a thick cylindrical bar due to longitudinal impact. JSME Int J Series A 39(1):60–70
22. Wilkins ML (1980) Use of artificial viscosity in multidimensional fluid dynamic calculations. J Comput Phys 36(3):281–303
23. Wilson EL, Farhoomand I, Bathe KJ (1973) Nonlinear dynamic analysis of complex structures. Earthq Eng Struct Dyn 1(3):241–252
24. Zhang GM, Batra RC (2007) Wave propagation in functionally graded materials by modified smoothed particle hydrodynamics (msph) method. J Comput Phys 222:374–390
25. Zienkiewicz OC, Taylor RL (2000) The finite element method. Butterworth-Heinemann, Oxford